Research Article | Vol. 25, No. 16 | 7 Aug 2017 | OPTICS EXPRESS 18566
Optics EXPRESS

Fano resonances in plasmonic heptamer nano-hole arrays

AKRAM HAJEBIFARD[1] AND PIERRE BERINI[1,2,3,*]

[1]Department of Physics, University of Ottawa, Ottawa K1N 6N5, Canada
[2]School of Electrical Engineering and Computer Sci., University of Ottawa, Ottawa K1N 6N5, Canada
[3]Centre for Research in Photonics at the University of Ottawa, Ottawa K1N 6N5, Canada
[*]berini@eecs.uottawa.ca

Abstract: The optical properties of gold heptamer nanohole arrays have been investigated theoretically and numerically. This structure support pronounced Fano resonances with high transmittance (~50%) and narrow bandwidths (down to 12 nm). The Fano features arise from the interference between light directly transmitted through the holes, and light indirectly scattered through the excitation of localized surface plasmon polaritons (LSPPs), propagating surface plasmon polaritons (SPPs), or/and waves related to Wood's anomaly (WA). The mechanisms behind the generation of these resonances are revealed by observing near-field distributions, altering the structural parameters and applying the Bloch wave model. Furthermore, it is shown that Fano resonances associated with LSPPs exhibit high surface (2 nm/nm) and bulk sensitivities (400 nm/RIU). However, the highest figure of merit (~24 RIU^{-1}) occurs for a Fano resonance involving a WA and SPP mode.

OCIS codes: (240.6680) Surface plasmons; (250.5403) Plasmonics; (280.4788) Optical sensing and sensors.

References and links

1. A. Otto, "Excitation of nonradiative surface plasma waves in silver by method of frustrated total reflection," Z. Phys. A: Hadrons Nucl. **216**(4), 398–410 (1968).
2. C. Wu, A. B. Khanikaev, R. Adato, N. Arju, A. A. Yanik, H. Altug, and G. Shvets, "Fano-resonant asymmetric metamaterials for ultrasensitive spectroscopy and identification of molecular monolayers," Nat. Mater. **11**(1), 69–75 (2011).
3. A. E. Cetin and H. Altug, "Fano resonant ring/disk plasmonic nanocavities on conducting substrates for advanced biosensing," ACS Nano **6**(11), 9989–9995 (2012).
4. N. A. Mirin, K. Bao, and P. Nordlander, "Fano resonances in plasmonic nanoparticle aggregates," J. Phys. Chem. A **113**(16), 4028–4034 (2009).
5. N. Liu, T. Weiss, M. Mesch, L. Langguth, U. Eigenthaler, M. Hirscher, C. Sönnichsen, and H. Giessen, "Planar metamaterial analogue of electromagnetically induced transparency for plasmonic sensing," Nano Lett. **10**(4), 1103–1107 (2010).
6. N. Verellen, Y. Sonnefraud, H. Sobhani, F. Hao, V. V. Moshchalkov, P. V. Dorpe, P. Nordlander, and S. A. Maier, "Fano resonances in individual coherent plasmonic nanocavities," Nano Lett. **9**(4), 1663–1667 (2009).
7. B. Gallinet and O. J. F. Martin, "Influence of electromagnetic interactions on the line shape of plasmonic Fano resonances," ACS Nano **5**(11), 8999–9008 (2011).
8. N. Papasimakis, Y. H. Fu, V. A. Fedotov, S. L. Prosvirnin, D. P. Tsai, and N. I. Zheludev, "Metamaterial with polarization and direction insensitive resonant transmission response mimicking electromagnetically induced transparency," Appl. Phys. Lett. **94**(21), 211902 (2009).
9. J. A. Fan, C. Wu, K. Bao, J. Bao, R. Bardhan, N. J. Halas, V. N. Manoharan, P. Nordlander, G. Shvets, and F. Capasso, "Self-assembled plasmonic nanoparticle clusters," Science **328**(5982), 1135–1138 (2010).
10. K. Thyagarajan, J. Butet, and O. J. F. Martin, "Augmenting second harmonic generation using Fano resonances in plasmonic systems," Nano Lett. **13**(4), 1847–1851 (2013).
11. F. Hao, Y. Sonnefraud, P. Van Dorpe, S. A. Maier, N. J. Halas, and P. Nordlander, "Symmetry breaking in plasmonic nanocavities: subradiant LSPR sensing and a tunable Fano resonance," Nano Lett. **8**(11), 3983–3988 (2008).
12. J. B. Lassiter, H. Sobhani, J. A. Fan, J. Kundu, F. Capasso, P. Nordlander, and N. J. Halas, "Fano resonances in plasmonic nanoclusters: geometrical and chemical tunability," Nano Lett. **10**(8), 3184–3189 (2010).
13. A. Christ, T. Zentgraf, J. Kuhl, S. Tikhodeev, N. Gippius, and H. Giessen, "Optical properties of planar metallic photonic crystal structures: Experiment and theory," Phys. Rev. B **70**(12), 125113 (2004).
14. A. Hajebifard and P. Berini, "Plasmonic Fano interference produced by gold nano-disks on a dielectric Bragg stack," J. Appl. Phys. **118**(9), 093107 (2015).

#287788 https://doi.org/10.1364/OE.25.018566
Journal © 2017 Received 2 Mar 2017; revised 25 May 2017; accepted 30 May 2017; published 24 Jul 2017

Optics EXPRESS

15. A. Christ, S. G. Tikhodeev, N. A. Gippius, J. Kuhl, and H. Giessen, "Waveguide-plasmon polaritons: strong coupling of photonic and electronic resonances in a metallic photonic crystal slab," Phys. Rev. Lett. **91**(18), 183901 (2003).
16. M. Svedendahl and M. Käll, "Fano interference between localized plasmons and interface reflections," ACS Nano **6**(8), 7533–7539 (2012).
17. I. Baryakhtar, Y. Demidenko, and V. Lozovski, "Interaction between localized-on-nanoparticles plasmon polaritons and surface plasmon polaritons," J. Opt. Soc. Am. B **30**(4), 1022–1026 (2013).
18. A. Artar, A. A. Yanik, and H. Altug, "Directional double Fano resonances in plasmonic hetero-oligomers," Nano Lett. **11**(9), 3694–3700 (2011).
19. G. F. Walsh and L. Dal Negro, "Enhanced second harmonic generation by photonic-plasmonic Fano-type coupling in nanoplasmonic arrays," Nano Lett. **13**(7), 3111–3117 (2013).
20. R. Near, C. Tabor, J. Duan, R. Pachter, and M. El-Sayed, "Pronounced effects of anisotropy on plasmonic properties of nanorings fabricated by electron beam lithography," Nano Lett. **12**(4), 2158–2164 (2012).
21. S. N. Sheikholeslami, A. García-Etxarri, and J. A. Dionne, "Controlling the interplay of electric and magnetic modes via Fano-like plasmon resonances," Nano Lett. **11**(9), 3927–3934 (2011).
22. J. A. Fan, K. Bao, C. Wu, J. Bao, R. Bardhan, N. J. Halas, V. N. Manoharan, G. Shvets, P. Nordlander, and F. Capasso, "Fano-like interference in self-assembled plasmonic quadrumer clusters," Nano Lett. **10**(11), 4680–4685 (2010).
23. J. A. Fan, Y. He, K. Bao, C. Wu, J. Bao, N. B. Schade, V. N. Manoharan, G. Shvets, P. Nordlander, D. R. Liu, and F. Capasso, "DNA-enabled self-assembly of plasmonic nanoclusters," Nano Lett. **11**(11), 4859–4864 (2011).
24. Y. Cui, J. Zhou, V. A. Tamma, and W. Park, "Dynamic tuning and symmetry lowering of Fano resonance in plasmonic nanostructure," ACS Nano **6**(3), 2385–2393 (2012).
25. M. Hentschel, M. Saliba, R. Vogelgesang, H. Giessen, A. P. Alivisatos, and N. Liu, "Transition from isolated to collective modes in plasmonic oligomers," Nano Lett. **10**(7), 2721–2726 (2010).
26. P. Alonso-Gonzalez, M. Schnell, P. Sarriugarte, H. Sobhani, C. Wu, N. Arju, A. Khanikaev, F. Golmar, P. Albella, L. Arzubiaga, F. Casanova, L. E. Hueso, P. Nordlander, G. Shvets, and R. Hillenbrand, "Real-space mapping of Fano interference in plasmonic metamolecules," Nano Lett. **11**(9), 3922–3926 (2011).
27. N. Liu, S. Kaiser, and H. Giessen, "Magnetoinductive and electroinductive coupling in plasmonic metamaterial molecules," Adv. Mater. **20**(23), 4521–4525 (2008).
28. J. Ye, F. Wen, H. Sobhani, J. B. Lassiter, P. Van Dorpe, P. Nordlander, and N. J. Halas, "Plasmonic nanoclusters: near field properties of the Fano resonance interrogated with SERS," Nano Lett. **12**(3), 1660–1667 (2012).
29. Z. Liu and J. Ye, "Highly controllable double Fano resonances in plasmonic metasurfaces," Nanoscale **8**(40), 17665–17674 (2016).
30. M. Alavirad, S. S. Mousavi, L. Roy, and P. Berini, "Schottky-contact plasmonic dipole rectenna concept for biosensing," Opt. Express **21**(4), 4328–4347 (2013).
31. R. Gordon, D. Sinton, K. L. Kavanagh, and A. G. Brolo, "A new generation of sensors based on extraordinary optical transmission," Acc. Chem. Res. **41**(8), 1049–1057 (2008).
32. L. Pang, G. M. Hwang, B. Slutsky, and Y. Fainman, "Spectral sensitivity of two-dimensional nanohole array surface plasmon polariton resonance sensor," Appl. Phys. Lett. **91**(12), 123112 (2007).
33. A. Lesuffleur, H. Im, N. C. Lindquist, K. S. Lim, and S.-H. Oh, "Laser-illuminated nanohole arrays for multiplex plasmonic microarray sensing," Opt. Express **16**(1), 219–224 (2008).
34. C. J. Alleyne, A. G. Kirk, R. C. McPhedran, N.-A. P. Nicorovici, and D. Maystre, "Enhanced SPR sensitivity using periodic metallic structures," Opt. Express **15**(13), 8163–8169 (2007).
35. Y. Zhan, D. Y. Lei, X. Li, and S. A. Maier, "Plasmonic Fano resonances in nanohole quadrumers for ultra-sensitive refractive index sensing," Nanoscale **6**(9), 4705–4715 (2014).
36. J. He, P. Ding, J. Wang, C. Fan, and E. Liang, "Double Fano-type resonances in heptamer-hole array transmission spectra with high refractive index sensing," J. Mod. Opt. **62**(15), 1241–1247 (2015).
37. S. H. Chang, S. Gray, and G. Schatz, "Surface plasmon generation and light transmission by isolated nanoholes and arrays of nanoholes in thin metal films," Opt. Express **13**(8), 3150–3165 (2005).
38. C. Genet, M. van Exter, and J. Woerdman, "Fano-type interpretation of red shifts and red tails in hole array transmission spectra," Opt. Commun. **225**(4-6), 331–336 (2003).
39. E. D. Palik, *Handbook of Optical Constants of Solids*, No. Book, Whole (Academic, 1997).
40. W. L. Barnes, W. A. Murray, J. Dintinger, E. Devaux, and T. W. Ebbesen, "Surface plasmon polaritons and their role in the enhanced transmission of light through periodic arrays of subwavelength holes in a metal film," Phys. Rev. Lett. **92**(10), 107401 (2004).
41. A. Hessel and A. A. Oliner, "A new theory of wood's anomalies on optical gratings," Appl. Opt. **4**(10), 1275–1297 (1965).
42. Z. Ruan and M. Qiu, "Enhanced transmission through periodic arrays of subwavelength holes: the role of localized waveguide resonances," Phys. Rev. Lett. **96**(23), 233901 (2006).
43. H. F. Ghaemi, T. Thio, D. E. Grupp, T. W. Ebbesen, and H. J. Lezec, "Surface plasmons enhance optical transmission through subwavelength holes," Phys. Rev. B **58**(11), 6779–6782 (1998).
44. J. A. Fan, C. Wu, K. Bao, J. Bao, R. Bardhan, N. J. Halas, V. N. Manoharan, P. Nordlander, G. Shvets, and F. Capasso, "Self-assembled plasmonic nanoparticle clusters," Science **328**(5982), 1135–1138 (2010).

Optics EXPRESS

45. M. Hentschel, T. Weiss, S. Bagheri, and H. Giessen, "Babinet to the half: coupling of solid and inverse plasmonic structures," Nano Lett. **13**(9), 4428–4433 (2013).
46. J. J. Burke, G. I. Stegeman, and T. Tamir, "Surface-polariton-like waves guided by thin, lossy metal films," Phys. Rev. B Condens. Matter **33**(8), 5186–5201 (1986).
47. P. Berini, "Plasmon-polariton waves guided by thin lossy metal films of finite width: Bound modes of asymmetric structures," Phys. Rev. B **63**(12), 125417 (2001).
48. J. M. McMahon, J. Henzie, T. W. Odom, G. C. Schatz, and S. K. Gray, "Tailoring the sensing capabilities of nanohole arrays in gold films with Rayleigh anomaly-surface plasmon polaritons," Opt. Express **15**(26), 18119–18129 (2007).
49. J. M. Steele, C. E. Moran, A. Lee, C. M. Aguirre, and N. J. Halas, "Metallodielectric gratings with subwavelength slots: Optical properties," Phys. Rev. B **68**(20), 205103 (2003).
50. T. Rindzevicius, Y. Alaverdyan, B. Sepulveda, T. Pakizeh, M. Kall, R. Hillenbrand, J. Aizpurua, and F. J. Garcia de Abajo, "Nanohole plasmons in optically thin gold films," J. Phys. Chem. C **111**(3), 1207–1212 (2007).
51. Y. Chu and K. B. Crozier, "Experimental study of the interaction between localized and propagating surface plasmons," Opt. Lett. **34**(3), 244–246 (2009).
52. N. Papanikolaou, "Optical properties of metallic nanoparticle arrays on a thin metallic film," Phys. Rev. B **75**, 235426 (2007).
53. T. Ohno, C. Wadell, S. Inagaki, J. Shi, Y. Nakamura, S. Matsushita, and T. Sannomiya, "Hole-size tuning and sensing performance of hexagonal plasmonic nanohole arrays," Opt. Mater. Express **6**(5), 1594–1603 (2016).
54. T. Sannomiya, O. Scholder, K. Jefimovs, C. Hafner, and A. B. Dahlin, "Investigation of plasmon resonances in metal films with nanohole arrays for biosensing applications," Small **7**(12), 1653–1663 (2011).
55. S. Zhang, L. Chen, Y. Huang, and H. Xu, "Reduced linewidth multipolar plasmon resonances in metal nanorods and related applications," Nanoscale **5**(15), 6985–6991 (2013).
56. H. Gao, J. M. McMahon, M. H. Lee, J. Henzie, S. K. Gray, G. C. Schatz, and T. W. Odom, "Rayleigh anomaly-surface plasmon polariton resonances in palladium and gold subwavelength hole arrays," Opt. Express **17**(4), 2334–2340 (2009).
57. G. A. Cervantes Tellez, S. Hassan, R. N. Tait, P. Berini, and R. Gordon, "Atomically flat symmetric elliptical nanohole arrays in a gold film for ultrasensitive refractive index sensing," Lab Chip **13**(13), 2541–2546 (2013).
58. A. E. Cetin, D. Etezadi, B. C. Galarreta, M. P. Busson, Y. Eksioglu, and H. Altug, "Plasmonic nanohole arrays on a robust hybrid substrate for highly sensitive label-free biosensing," ACS Photonics **2**(8), 1167–1174 (2015).
59. A. Hajiaboli, M. Kahrizi, and T. Vo-Van, "Optical behaviour of thick gold and silver films with periodic circular nanohole arrays," J. Phys. - Appl. Phys. (Berl.) **45**, 485105 (2012).

1. Introduction

Compared to the symmetric Lorentzian lineshape supported in various nanostructures [1], asymmetric Fano resonances in plasmonic structures have recently attracted intense attention [2,3] due to their remarkable characteristics such as a narrow asymmetric line-shape, strong electromagnetic field enhancement, light confinement to the nanometer scale, and high spectral sensitivity to changes in the local dielectric environment [1,4–6]. In plasmonic structures, Fano resonances originate from the interference between light directly coupled to a bright mode (continuum), and light indirectly coupled to a dark mode (subradiant) excited via near-field interactions with the bright mode [7]. A Fano peak is a consequence of constructive interference between such modes, whereas a Fano dip arises as the two modes interfere destructively such as when the dark mode is out of phase with respect to the continuum. Taking advantage of this principle, different types of plasmonic structures, such as metamaterials [5,8], clusters [9,10], single and multi-surface nanoparticles [11,12] and periodic structures [13–17] have been proposed and studied, seeking Fano resonances in their spectral responses. Structures generating pronounced Fano resonances include assemblies of plasmonic nanoparticles, such as dimers [18–20], trimers [21], quadrumers [22], pentamers [23] and heptamers [10,24–26], where various parameters such as inter-particle separation and particle size can be tuned, but also symmetry can be broken, to tailor the characteristics of Fano resonances.

Unlike plasmonic nanoparticle assemblies, far less attention has been paid to complementary structures - arrangement of metallic nanoholes - which are also expected to support Fano resonances [5,27]. We show that arrangements of nanoholes in metal films produce more complex spectral responses because the structure supports many excitations, including localised surface plasmon polaritons (LSPPs) in the vicinity of holes, and propagating surface plasmon polaritons (SPPs) or Wood's anomaly (WA) waves excited on

Optics EXPRESS

the metal film that also interact with the holes. In comparison with complementary structures, the increased number of modes in metallic nanohole assemblies suggests broadband interrogation to track multiple resonances, resulting in improvement of the detection limit and measurement accuracy. Also, the increased number of resonances, and the ability to independently tune the position of SPP and LSPP resonances (both providing near-field enhancement) is favorable for double-resonance SERS applications, where simultaneous enhancement at both the excitation and Stokes wavelengths is needed [28,29].

In addition, compared to complementary structures where interconnections between nanoantennas are required for, *e.g.*, optoelectronic applications, the continuity of the metallic layer in the nanohole arrangements can be useful for producing, *e.g.,* resonant Schottky contacts [30]. Finally, nanohole arrays as biosensors allow for a high degree of multiplexing, parallel optical detection, and the ability to integrate microfluidics [31–34]. Recently, some research has been focused on plasmonic nanohole clusters, such as individual nanohole quadrumers [35], and arrays of heptamer-arranged nanoholes [36], but this area of study remains largely unexplored. The purpose of this paper is to investigate the optical properties of arrays of heptamer-arranged nanoholes (HNH) in detail, offer physical interpretations for the generation of Fano resonances in such arrays, and consider their application to biosensors. Heptamer-arranged nanoholes form a plasmonic oligomer consisting of one nanohole surrounded by six others forming a high packing density arrangement of nanoholes, which produces many hot spot areas between neighboring elements. Also the high spatial symmetry of HNH simplifies polarization alignments and facilities interrogation.

We numerically study arrays of HNH drilled into a thin gold film on a SiO_2 substrate covered by different superstrate media, which renders the structure asymmetric and rich in excitations and spectral features. We also investigate in detail the effects caused by changing the geometrical parameters, including periodicity, metal thickness, inter-hole distance and the radius of the central hole in the heptamer, and we connect the numerical results to an analytical Bloch wave model. The sensitivity of the Fano features to small changes in the refractive index (RI) of the superstrate medium makes the structure a potential candidate for chemical and biological sensors. We thus also examine the device for use as a biosensor by calculating the bulk sensitivity, the Figure of Merit (FoM) and the surface sensitivity. We find that the proposed structure supports pronounced Fano resonances in the near infrared (NIR) range of the optical spectrum. Four types of modes, consisting of LSPPs and propagating symmetric SPP (SPP_s), asymmetric SPP (SPP_a) and WA waves play essential roles in the formation of Fano resonances. The Fano resonances arise from the interference between the light transmitted directly through the holes (continuum) and the light indirectly scattered due the excitation of these four types of modes [37,38].

2. Proposed structure and numerical model

Figure 1 shows schematically the structure under study, which is an array of HNH in a thin Au film supported by a SiO_2 substrate and covered by a dielectric medium (several considered). The geometrical parameters including the metal thickness (t), inter-hole gap (G), periodicity of the array ($P = P_y = P_z$), and diameter of the central hole (D_c) are varied, but the diameter of holes on the outer ring (D) remains fixed. Transmittance (T), reflectance (R) and absorptance (A = 1 - R - T) spectra are calculated as the response of the structure, because each might be useful based on the potential applications of the system. For instance, the absorptance is required for SERS and Schottky contact photodetector applications [28,30], whereas the transmittance and reflectance are useful for biosensing applications [31]. Throughout the paper, absorptance peaks are used to identify the position of resonances. To compute the spectra and the associated electromagnetic fields, the structure was modeled using a commercial (COMSOL) implementation of the finite element method (FEM), solving the vector wave equations for the E and H field vectors throughout the structure, subject to the applicable boundary conditions, and the applied source fields. The structure was meshed

Optics EXPRESS

using tetrahedral mesh elements with a resolution between 5 and 12 nm in the gold film, while the mesh size was increased gradually away from the gold film with a maximum mesh element size of 100 nm. Taking advantage of the structural symmetry, only one unit cell incorporating one heptamer arrangement of nanoholes was modelled. To do so, periodic boundary conditions were applied on the lateral walls and absorbing boundary conditions on the front and back walls. The structure was then illuminated by y- and z-polarized electromagnetic waves perpendicularly incident onto the structure from the substrate side. The optical properties of the materials were taken as the wavelength-dependent complex refractive index measured over the range of interest for SiO_2 [39] and Au [40]. Cubic spline interpolation functions were applied to determine the refractive indices at some wavelengths of interest where data were not available.

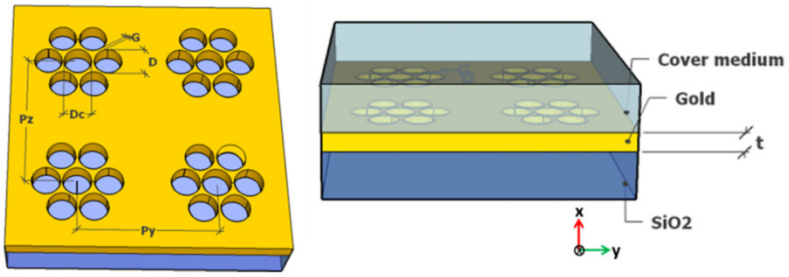

Fig. 1. Schematic of an HNH array on a SiO_2 substrate, and covered by a superstrate medium. The geometrical parameters include, metal thickness (t), inter-hole gap (G), periodicity of the array ($P = P_y = P_z$), and the diameter of the central holes (D_c) and of the surrounding holes (D).

3. Results and discussions

Considering the HNH array as a grating of lattice constant $P = P_y = P_z$ illuminated by light incident at an angle θ, the light gains additional momentum given by $|G_y| = |G_z| = 2\pi/P$, which can excite propagating SPP modes (Bloch waves) on the metal film following the Bragg coupling condition [41]:

$$K_{spp} = K_0 \sin\theta + S_y G_y + S_z G_z \quad (1)$$

In addition to SPP modes guided by the metal film, the grating effect of the HNH array can launch WA waves, which are associated with light diffracted parallel to the surface of the structure, excited under the following condition [37,41]:

$$K_{WA} = K_0 \sin\theta + W_y G_y + W_z G_z \quad (2)$$

In the above, k_0, k_{SPP} ($= k_0 n_{SPP}$) and k_{WA} ($= k_0 n_d$) are the wavenumbers of free-space, of the SPP mode (symmetric or asymmetric) excited and guided by the thin metal film, and of WA waves, respectively. nd is the refractive index of the medium in which the WA wave travels, nSPP is the effective mode index of an SPP mode, which is defined as $n_{spp} = \beta/k_0$ and $\beta = \beta' + i\beta''$ is the propagation constant of the mode. The integer index pairs (S_y, S_z) and (W_y, W_z) denote the diffraction order and are included in our nomenclature; for example, $SPP_a(1,0)$ and $SPP_s(1,1)$ refer to the asymmetric SPP propagating along the y axis, and the symmetric SPP along the diagonal to the y and z axes, respectively. For the case of normal incidence, Eqs. (1) and (2) can be rewritten as follows, in terms of the SPP wavelengths (λ_{SPP}) and WA wavelengths (λ_{WA}) [42,43]:

$$\lambda_{SPP} = \frac{P}{(S_y^2 + S_z^2)^{1/2}} n_{SPP} \quad (3)$$

Optics EXPRESS

$$\lambda_{WA} = \frac{P}{(W_y^2 + W_z^2)^{1/2}} n_d \quad (4)$$

Equations (1)-(4) are approximate for our HNH arrays, because they hold for small perturbations whereas our arrays produce strong perturbations. The array of HNH not only operates as a diffraction grating to excite SPP modes supported by the metal film, or WA waves in either the substrate or superstrate, but it can also support LSPP resonances within the cluster of holes. A cluster of plasmonic nanoholes (or nanoparticles) can support coupled plasmon modes which are combinations of the plasmon modes supported by each constituent hole (nanoparticle) for sufficiently small inter-hole (inter-particle) separations [8,44]. It is expected that the HNH structure supports some Fano features arising from the interference between light directly transmitted through the holes, and light indirectly scattered through the excitation of LSPPs, propagating SPPs, or/and waves related to Wood's anomaly (WA).

3.1 Optical responses of HNH array

The optical responses of a HNH array, for both y- (black line) and z-(red line) linearly-polarized incident light, are shown in Fig. 2, which illustrates several Fano features. The HNH array includes holes with diameters of $D = D_c = 100$ nm and inter-hole distances of $G = 10$ nm in a gold film of thickness $t = 60$ nm, supported by SiO_2 substrate and covered by a dielectric material of refractive index $n_s = 1.33$. The periodicity was set to $P = P_y = P_z = 480$ nm, and the wavelength varied from 630 nm to 1000 nm. As shown in Fig. 2(b), the structure supports four Fano resonances for y-polarized incident light (black curve), at $\lambda_{1y} = 644$ nm, $\lambda_{2y} = 700$ nm, $\lambda_{3y} = 780$ nm and $\lambda_{4y} = 884$nm, denoted as $SPP_a(1,1)$, WA-$SPP_s(1,0)$, $SPP_a(1,0)$ and $LSPP_1$, respectively.

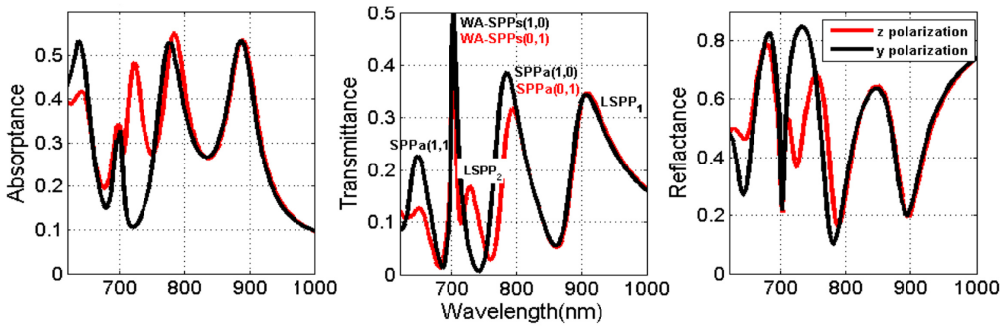

Fig. 2. Optical response of an array of HNH, for y-polarized (black curves) and z-polarized (red curves) incident light. The structure supports several Fano resonances denoted as $SPP_a(1,1)$, WA-SPP_s, $LSPP_2$, $SPP_a(1,0)$ and $LSPP_1$.

Also it supports five Fano resonances for z-polarized incident light (red curve), at $\lambda_{1z} = 642$ nm, $\lambda_{2z} = 698$ nm, $\lambda_{3z} = 721$ nm, $\lambda_{4z} = 785$ nm and $\lambda_{5z} = 886$ nm, denoted as $SPP_a(1,1)$, WA-$SPP_s(1,0)$, $LSPP_2$, $SPP_a(1,0)$ and $LSPP_1$, respectively. The physical mechanisms behind the formation of these resonances can be revealed by observing near electromagnetic field distributions, by changing the geometrical parameters of the structure, and also by considering the Bloch wave model.

3.2 Electromagnetic near-field distributions

To understand the mechanism behind the generation of each Fano resonance in the HNH array, electric and magnetic near-field distributions in a unit cell were computed at the spectral position of the resonances. The electric field amplitude of the incident wave was set to 1 V/m, so the electric field plots show directly the field enhancement. The electric field intensity (|E|), the x-component (perpendicular) of electric field (E_x), the x component of

Optics EXPRESS

magnetic field (H_x), and the y or z component of magnetic field (H_y or H_z) are shown in Fig. 3, for y-polarized incident light, and in Fig. 4, for z-polarized incident light. According to the Babinet's principle, resonances in a complementary structure are associated with the magnetic moment [45] which is revealed by H_x field distributions in this structure. Also, based on this principle, H_y or H_z magnetic field profiles can be provided to illustrate the propagating and localized surface plasmons. Based on the electromagnetic near-field distributions, the Fano resonances can be categorized as LSPP Fano resonances or propagating SPP Fano resonances.

3.2.1 LSPP Fano resonance

The near-field distribution of |E|, of the Fano resonances at λ_{4y} = 884nm and λ_{5z} = 886 nm, shown in Figs. 3 (a4) and 4 (a5), reveals that the corresponding fields are strongly localized to the center of the unit cell, which is a typical feature of a LSPP mode. A dipolar pattern in the HNH structure is seen in the H_x field distribution provided in Figs. 3(d4) and 4(d5). Based on the H_x distribution, this LSPP mode, which is called LSPP1, arises from anti-bonding hybridization between the central and surrounding ring holes, in which the central hole shows a notable magnetic dipole oscillating out of phase with respect to the dipole of the six surrounding holes, forming an antibonding coupled plasmon mode. A higher order LSPP mode, $LSPP_2$, which is excited by a z-polarized incident field, and occurring at λ_{3z} = 721 nm, shows a strong |E| field localization near to the surrounding holes of the unit cell. Based on the corresponding H_x field distribution shown in Fig. 4(d3), $LSPP_2$ mode arises from the hybridization between the magnetic multipolar plasmon of the central hole and the magnetic dipolar plasmon of the six surrounding holes.

3.2.2 Propagating SPP Fano resonances

In a thick metal film, two independent single-interface SPP modes can be supported on opposite sides. However in the case of a thin metal film, these two SPP modes are coupled to each other, forming one lower energy symmetric supermode (often termed the sb mode [46] denoted herein as SPP_s) and one higher energy asymmetric supermode (often termed the ab mode, denoted herein as SPP_a). In terms of field distribution, both of them show a maximum |E| at the metal-dielectric interfaces and decay exponentially away. In the case of the symmetric mode, the transverse electric field (E_x here) doesn't go through zero inside the metal film so this field component doesn't change in sign from one interface to the other. Conversely, E_x for the asymmetric mode goes through zero inside the metal film and changes sign from one interface to the other [47].

(*i*) $SPP_a(1,0)$ and $SPP_a(0,1)$: For the resonances at λ_{3y} = 780 nm and λ_{4z} = 785 nm (Fig. 2), the electric field distributions, plotted in Figs. 3 (a3) and 3(b3), and in Figs. 4(a4) and 4(b4) reveal the characteristics of an asymmetric SPP propagating along the metal film. The corresponding H_z field distribution shown in Fig. 3(e3) and H_y field distributions in Fig. 4 (e4) show the propagation of the SPP_a mode in the y direction for the y polarized incident light, and z direction for the z polarized incident light, respectively. Conclusively, these resonances are termed $SPP_a(1,0)$ and $SPP_a(0,1)$.

Optics EXPRESS

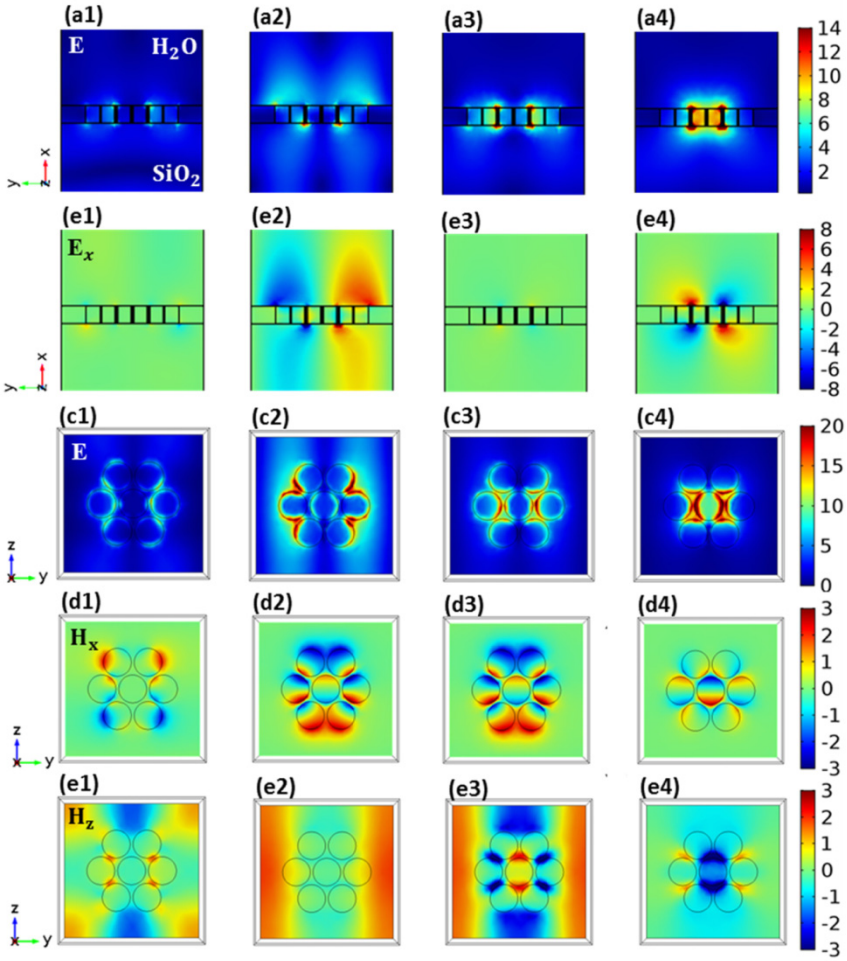

Fig. 3. Near-field distribution of |**E**| at (a1) λ_{1y}, (a2) λ_{2y}, (a3) λ_{3y} and (a4) λ_{4y}, and near-field distribution of E_x at (b1) λ_{1y}, (b2) λ_{2y}, (b3) λ_{3y} and (b4) λ_{4y}, along the xy plane passing through the center of a unit cell. Near-field distribution of |**E**| at (c1) λ_{1y}, (c2) λ_{2y}, (c3) λ_{3y} and (c4) λ_{4y}, near-field distribution of H_x at (d1) λ_{1y}, (d2) λ_{2y}, (d3) λ_{3y} and (d4) λ_{4y}, and near-field distribution of H_z at (e1) λ_{1y}, (e2) λ_{2y}, (e3) λ_{3y} and (e4) λ_{4y}, along the yz plane at the Au/cover interface. All fields were computed for y-polarized incident light on resonance where λ_{1y} = 644 nm, λ_{2y} = 700 nm, λ_{3y} = 780 nm, and λ_{4y} = 884 nm (*cf*. Figure 2).

(*ii*) WA-SPP_s(1,0) and WA-SPP_s(0,1): The narrowest resonances occur at λ_{2y} = 700 nm and λ_{2z} = 699 nm and are due to the coupling of a WA wave on one side of the metal film with the SPP_s mode [48]. The electric field distributions, plotted in Figs. 3 (b2) and 4(b2), reveal the excitation of the symmetric SPP mode, and also the excitation of WA waves in the SiO_2 as an extended plane wave propagating parallel to the metal film [49]. The corresponding field distributions of H_z, shown in Fig. 3(e2) and H_y shown in Fig. 4(e2), show the propagation of the WA-SPP_s mode in the y direction for the y polarized incident light, and z direction for the z polarized incident light, respectively. Conclusively, these resonances are labelled WA-SPP_s(1,0) and WA-SPP_s(0,1).

(*iii*) SPP_a(1,1): The shortest wavelength resonances observed, at λ_{1y} = 644 nm and λ_{2z} = 642 nm, are due to the excitation of the asymmetric SPP mode along the (1,1) direction. The electric field distributions, plotted in Figs. 3 (a1) and 3(b1), and in Figs. 4(a1) and 4(b1), reveal the excitation of this mode. Furthermore, the corresponding H_z shown in Fig. 3 (e1)

Optics EXPRESS

and H_y shown in Fig. 4 (e1) exhibit a diagonal standing wave pattern due to the propagation of the $SPP_a(1,1)$, corresponding to a second order diffraction.

The near-field distribution of |**E**| on the yz plane at the cover/Au interface is shown in row c of Figs. 3 and 4, showing the electric field enhancement and hot spots that are useful for SERS applications. The highest field enchantment (up to 29) is localized near the central hole of the HNH and observed for the LSPR mode (Figs. 3(c4) and 4(c5)).

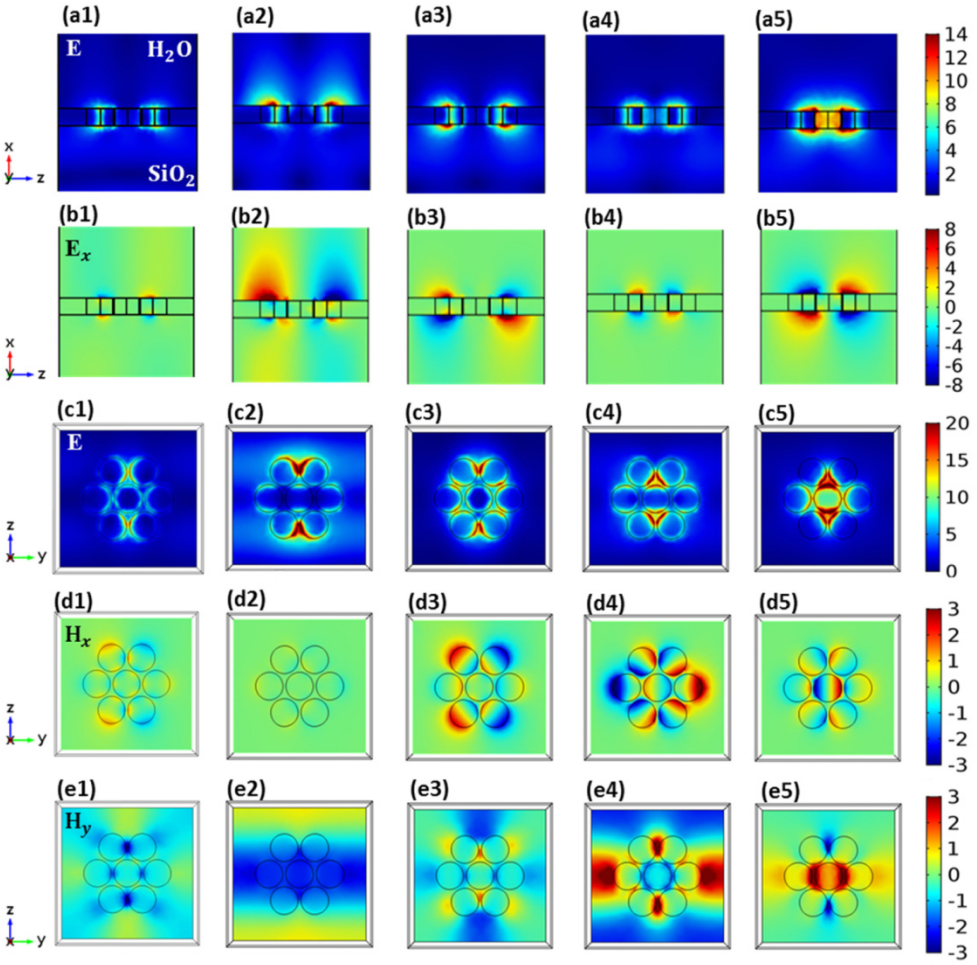

Fig. 4. Near field distribution of |**E**| at (a1) λ_{1z}, (a2) λ_{2z}, (a3) λ_{3z}, (a4) λ_{4z} and (a5) λ_{5z}, and near field distribution of E_x at (b1) λ_{1z}, (b2) λ_{2z}, (b3) λ_{3z}, (b4) λ_{4z} and (b5) λ_{5z}, along the xz plane passing through the center of a unit cell. Near-field distribution of |**E**| at (c1) λ_{1z}, (c2) λ_{2z}, (c3) λ_{3z}, (c4) λ_{4z} and (c5) λ_{5z}, near-field distribution of H_x at (d1) λ_{1z}, (d2) λ_{2z}, (d3) λ_{3z}, (d4) λ_{4z} and (d5) λ_{5z}, and near-field distribution of H_y at (e1) λ_{1z}, (e2) λ_{2z}, (e3) λ_{3z}, (e4) λ_{4z} and (e5) λ_{5z} along the yz plane at the Au/cover interface. All fields were computed for z-polarized incident light on resonance where λ_{1z} = 642 nm, λ_{2z} = 698 nm, λ_{3z} = 721 nm, λ_{4z} = 785 nm, and λ_{5z} = 886 nm (*cf.* Fig. 2).

According to the electric and magnetic near-field distributions in Fig. 3-Fig. 4, the Fano resonances can be categorized as resonances related to the excitation of LSPPs - fields are strongly localized about the heptamer, SPPa - fields propagate along the metal-dielectric interfaces (E_x is asymmetric), and WA-SPPs - fields also propagate, revealing the excitation of the SPPs and WA on opposite sides of metal film, along with coupling of these waves (E_x is symmetric).

Optics EXPRESS

3.3 Geometrical and dielectric parameters

3.3.1 Geometrical parameters

Changing the geometrical parameters of the system and observing the evolution of the Fano resonances provides further insight into their nature and formation. Here, for simplicity, we consider only the case of y-polarized incident light. The dependences of the spectra on the periodicity (440 < P < 520 nm), the central hole's diameter (40 < Dc < 100 nm), the inter-hole separation (10 < G < 30 nm) and the thickness of the metal film (30 < t < 60 nm) are plotted in Figs. 5(a)-5(d), respectively. In Fig. 5, the Fano resonances associated with the LSPP1, and the propagating SPPa(1,0) and WA-SPPs(1,0) modes are indicated by yellow, black and red dashed lines on the absorptance spectra, respectively. The SPP-related Fano resonances are not only sensitive to the array periodicity P, but also to the metal thickness t and the full size of the aperture (which depends on Dc and G in our case) presented by the holes [47,50]. The LSPPs-Fano resonance depends primarily on the HNH parameters.

(*i*) $SPP_a(1,0)$: The resonance red-shifts with increasing pitch P, as anticipated by Eq. (3), and observed in Fig. 5(a). Increasing t decreases the effective index (n_{spp}) of the SPP_a mode, which based on Eq. (3) causes the associated Fano resonance to blue-shift, as observed in Fig. 5(d). However, as shown in Fig. 5(b), changing D_c has little effect on the position of this resonance - the blue shift for the specific case of D_c = 80 nm is due to the merging and strong coupling with the $LSPP_1$ Fano resonance, resulting in a repulsive behavior between these two resonances [51,52]. Conversely, increasing G from 10 to 30 nm results in increasing the full size of the aperture from 320 to 360 nm, leading to a blue-shift in the resonance [53,54].

(*ii*) WA-$SPP_s(1,0)$: This Fano resonance involves the SPP_s coupled to a WA wave. The constituent WA wave is mainly influenced by the periodicity P, following Eq. (4), but the constituent SPP_s mode is influenced by the same factors as the SPP_a mode (the periodicity P following Eq. (3), the film thickness t and the full size of the aperture). The resonance red-shifts with increasing pitch P, as anticipated by Eqs. (3) and (4), as observed in Fig. 5(a). Increasing t from 30 to 60 nm (range of t over which the WA-SPP can exist) [48], increases the effective index (n_{spp}) of the constituent SPP_s mode, which based on Eq. (3), causes the associated Fano resonance to red-shift, as observed in Fig. 5(d) (opposite direction to the $SPP_a(1,0)$ resonance). Changing D_c has little effect on the resonance, as observed in Fig. 5(b), whereas increasing G increases the full size of the aperture, leading to a blue-shift in the resonance as observed in Fig. 5(c). The shift is in the same direction as the $SSP_a(1,0)$ mode but is weaker due to the lower confinement of the SPP_s mode to the metal film.

(*iii*) $LSPP_1$: The Fano resonance associated with the $LSPP_1$ is dependant primarily on the size of the holes D_c and the separation between holes G, but not much on the periodicity P as observed in Fig. 5. Unlike the SPP_a and WA-SPP_s Fano resonances, the $LSPP_1$ resonance arises from the anti-bonding hybridization between the central and surrounding holes, so it is affected strongly by the geometry of these features but not much by the pitch as observed in Fig. 5(a). This resonance exhibits a significant red shift of ~200 nm by increasing D_c from 40 to 100 nm. Meanwhile, increasing G shifts the resonance towards the blue, as observed in Fig. 5(c). The $LSPP_1$ is also sensitive to the metal thickness as changing the latter from t = 30 to 60 nm causes a blue-shift.

In summary, we observe the evolution of the Fano resonances with changes in the structural parameters of the system in Fig. 5, which helps elucidate their character. As predicted by Eqs. (3) and (4), this figure illustrates that the WA-SPP and SPP-related Fano resonances are sensitive to the array periodicity P, however, the LSPP-related Fano resonances are not. In addition, as expected, the LSPP Fano resonance is affected strongly by the central hole's diameter, whereas changing this parameter doesn't affect the other resonances. As seen in Fig. 5(d), increasing the metal thickness decreases and increases the effective index of the SPP_a and SPP_s mode, respectively, producing a blue-shift in the resonance associated with the former and a red-shift for the latter.

Optics EXPRESS

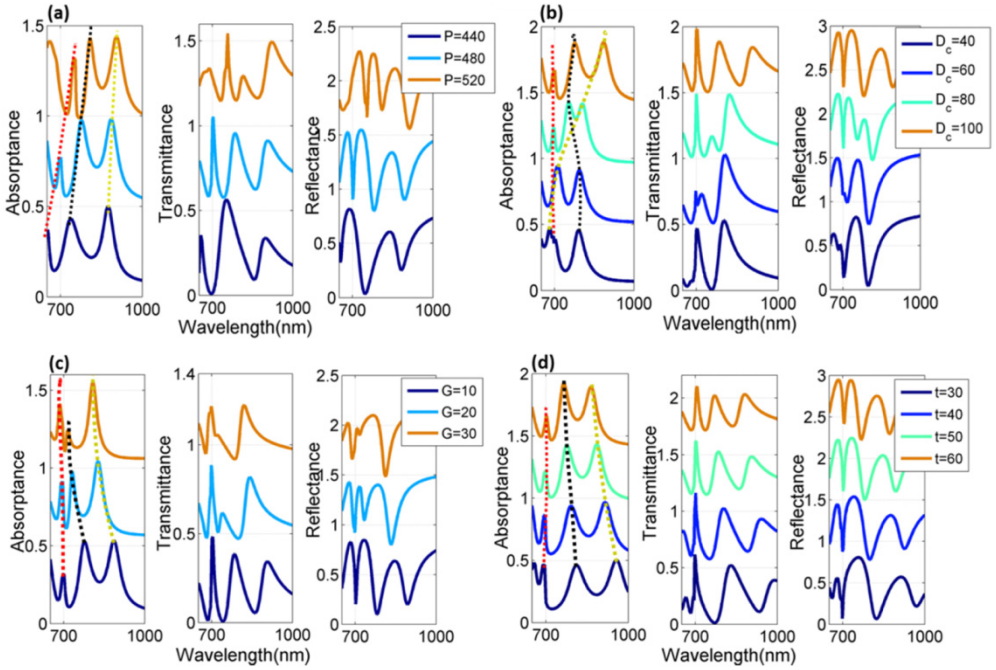

Fig. 5. Optical responses of the HNH arrays for the geometrical parameters of: (a) D = D_c = 100 nm, G = 10 nm, t = 60 nm and various P; (b) D = 100 nm, G = 10 nm, t = 60 nm, P = 480 nm, and various D_c; (c) D = D_c = 100 nm, t = 60 nm, P = 480 nm, and various G; (d) D = D_c = 100 nm, G = 10 nm, P = 480 nm, and various t. Spectra in (a)-(d) are offset vertically for clarity. The Fano resonances associated with the $LSPP_1$, and the propagating SPP_a and WA-SPP_s modes are indicated by yellow, black and red dashed lines, respectively.

3.3.2 Dielectric parameters

The dependence of the Fano resonances on the refractive index of the cover medium n_s is plotted in Fig. 6 (a). This figure shows the optical responses of an array of HNH with the geometrical parameters D = D_c = 100 nm, G = 10 nm, t = 60 nm, and P = 480 nm, sandwiched between SiO_2 as the substrate and a medium of $1.33 < n_s < 1.49$ as the cover. As observed in the transmittance spectra shown in Fig. 6 (b), all resonances are sensitive to n_s and they all shift to longer wavelengths as n_s increases. In this figure, the resonances are identified as $SPP_a(1,1)$, $SPP_s(1,0)$, WA-$SPP_s(1,0)$, $SPP_a(1,0)$ and $LSPP_1$. The narrowest resonance, WA-$SPP_s(1,0)$ (tracked by red arrows), experiences a rapid rise and narrowing with decreasing n_s. This rapid change is the direct result of a more effective coupling between the WA(1,0) in SiO_2 and the $SPP_s(1,0)$ localized along the Au/cover interface. According to Eq. (4), the first diffraction order of the WA wave in SiO_2, WA(1,0), occurs at = 697 nm. By increasing n_s, the spectral position of the $SPP_s(1,0)$ mode moves away from WA(1,0), so the coupling between these two waves decreases, which results in increased damping of this resonance for $n_s > 1.41$. For higher n_s, the coupled WA-$SPP_s(1,0)$ excitation no longer exists, so the $SPP_s(1,0)$ mode becomes independent (tracked by pink arrows).

3.4 Bloch wave model

More insight on the generation of the Fano resonances can be gained by using Eqs. (1)-(4), along with modal results, to anticipate the spectral position of the resonances associated with propagating SPP modes. As mentioned earlier, a thin metal film supports two bound coupled modes termed the symmetric SPP (SPP_s) and asymmetric SPP (SPP_a). In Fig. 7 (a), the effective index of SPP_a (dash-dot lines) and SPP_s (dash lines) modes are plotted as a function of wavelength for a gold film 60 nm thick, while n_s increases from 1.33 to 1.49. Inserting the

Optics EXPRESS

calculated effective indices in Eqs. (1) and (3), with P = 480 nm, the grating dispersion relation for the SPP_a (dash-dot blue) and SPP_s (dash blue) modes are plotted in Fig. 7(b) for the specific case of $n_s = 1.41$. At normal incidence (k = 0), the dispersion curves anticipate the excitation of the SPP_s mode at = 698 nm and of the SPP_a mode at λ = 745 nm. This is in reasonably good agreement with the results of Fig. 6, where these resonances occur at λ = 725 nm and λ = 800 nm, respectively, ~25 and ~50 nm away from what the dispersion curve anticipates - the origin of the discrepancies is that the HNH array is not a weak perturbation for which Eqs. (1) and (3) hold.

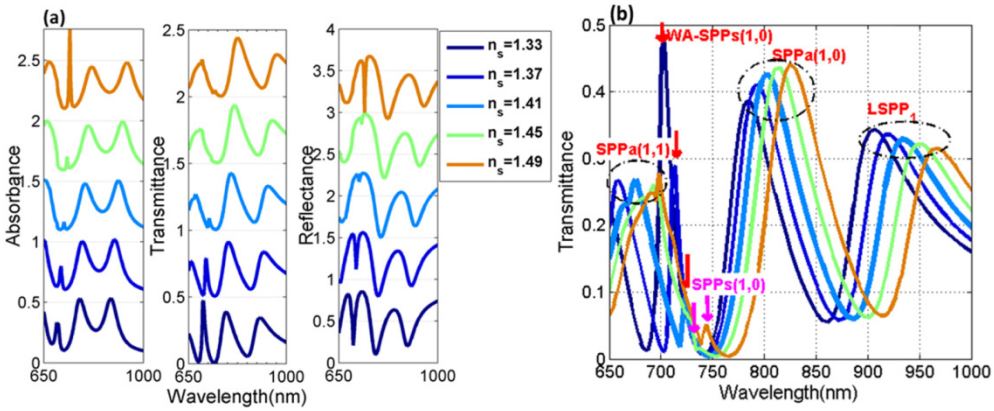

Fig. 6. (a) Optical responses of the HNH array for various cover medium's refractive index. Spectra are offset vertically for clarity. (b) Superimposed transmittance spectra of the array highlighting the shift in the $LSPP_1$, $SPP_a(1,0)$, $SPP_a(1,1)$ Fano resonances and the evolution of the $WA\text{-}SPP_s(1,0)$ and $SPP_s(1,0)$ Fano resonances (red and pink arrows, respectively).

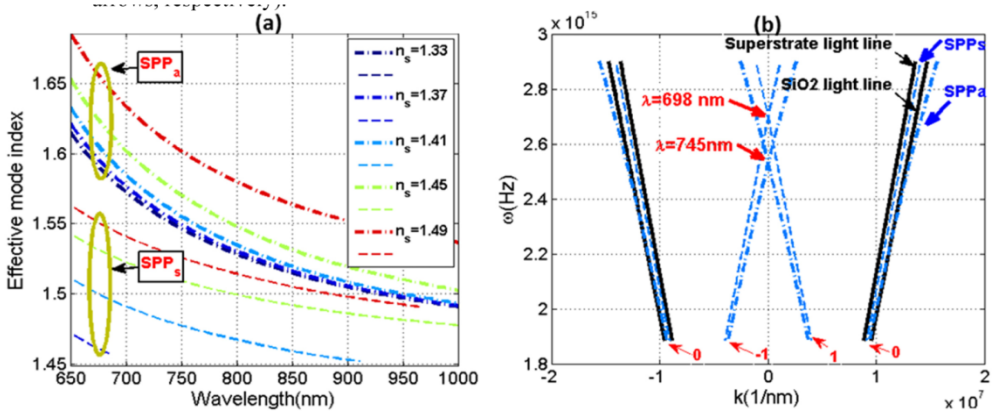

Fig. 7. (a) Effective index *vs*. wavelength for the SPP_a (dash-dot) and SPP_s (dash) modes on an Au film of t = 60 nm with n_s varying from 1.33 to 1.49. (b) Grating dispersion of the SPP_a (blue dash-dot) and SPP_s (blue dash) modes for $n_s = 1.41$ and P = 480 nm. The solid black lines are the light lines in SiO_2 and in the cover medium ($n_s = 1.41$). At normal incidence (k = 0), the dispersion curves anticipate the excitation of the SPP_s mode at λ = 698 nm and of the SPP_a mode at λ = 745 nm. The dispersion curves for the −1, 0, + 1 diffraction orders are also shown on the figure.

3.5 Sensing performance

As shown in Fig. 6, the Fano resonances of the HNH array are very sensitive to n_s which suggests application of the structure to refractive index sensing, particularly biochemical sensing. To characterize the sensing performance of a structure, the refractive index sensitivity (bulk sensitivity - BS), figure of merit (FoM) and surface sensitivity (SS) were

Optics EXPRESS

calculated. The bulk sensitivity is defined as the shift in a resonant wavelength relative to the change in the refractive index of the cover medium and the FoM is defined as the bulk sensitivity divided by the spectral linewidth. Following conventions in previous work [11,16,22,55], the spectral linewidth for an asymmetric resonance like a Fano resonance is taken as the wavelength difference between the Fano dip and the adjacent peak. The surface sensitivity is defined as the shift in λ_{res} relative to the change in the adlayer thickness (a), for an adlayer growing at the Au/cover interface. In the following, these sensitivities were calculated for an HNH array having D = D_c = 100 nm, G = 10 nm, t = 60 nm, P = 480 nm, assuming SiO_2 as the substrate and a cover medium of refractive index n_s = 1.33 (*e.g.*, H_2O). Results were obtained for both y- and z- polarized incident light.

3.5.1 Bulk sensitivity

Figure 8 (a) shows how the Fano resonances in the transmitted spectrum red-shift with small changes in cover refractive index (Δn_s = 0.01) for the case of y-polarized incident light. The wavelength shift relative to the nominal resonance wavelength of the modes at n_s = 1.33 is plotted *vs*. the cover refractive index in Fig. 8 (b). As indicated on this figure, the $LSPP_1$, $SPP_a(1,0)$ and WA-$SPP_s(1,0)$ Fano resonances produce bulk sensitivities of 400, 200 and 250 nm/RIU, respectively, while their FoM values are 4.71, 3.78 and 23.8 RIU^{-1}, respectively. The $LSPP_1$ Fano resonance produces the largest bulk sensitivity because the electromagnetic field of this mode is highly localized to the holes, where the sensing medium penetrates. In addition, the WA-$SPP_s(1,0)$ Fano resonance exhibits the highest FoM because it has the sharpest resonance. For z-polarized incident light, the evolution of the Fano resonances is plotted in Figs. 9 (a), and 9 (b) shows the shift in resonance wavelength with respect to their nominal values at n_s = 1.33 *vs*. the cover refractive index. The bulk sensitivity and FoM associated with each Fano resonance is also given.

Compared to studies on arrays of individual nanoholes of similar geometry as our HNH, the HNH array provides improved bulk sensitivity and FoM values [48,56,57], and a higher transmittance (~50%) [40,48,58,59], resulting in higher intensity signals at the detector, improvement of signal to noise ratio, and limit of detection. Complementary structures - arrays of heptamer-arranged nanoparticles (HNP) - can only support $LSPP_1$ Fano resonances due to the absence of a waveguide and propagating modes, so spectra are not as rich in features. Our arrays of HNH compare well to arrays of HNP of similar dimensions. For instance, arrays of Au heptamer nano-disks with G = 15 nm, D = D_c = 128 nm and t = 30 nm, produce a bulk sensitivity of 428 nm/RIU and FoM of 5.1 RIU^{-1} [12], which corresponds to nearly the same performance as our HNH structures. For arrays of Ag heptamer nano-spheres with G = 5 nm and D = D_c = 100 nm on SiO_2, the $LSPP_1$ Fano resonance produces a bulk sensitivity of 514 nm/RIU and FoM of 10.6 RIU^{-1} [4], which are higher than our values for the HNH structure. The better bulk sensitivity is due to an inter-particle distance that is smaller than in our HNH and to the sensing medium being air rather than water. Also their spheres are made of Ag which has better optical parameters than Au (the former is reactive).

Optics EXPRESS

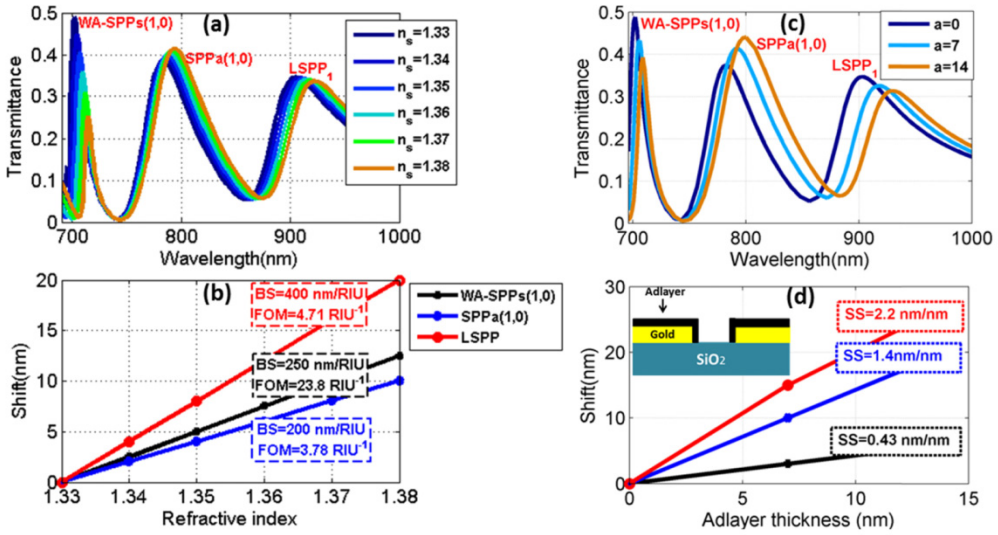

Fig. 8. Transmittance spectra of the HNH array illuminated with a y-polarized incident light, (a) while n_s changing. (b) Shift in the resonance wavelengths with respect to their nominal values at n_s = 1.33 *vs*. the superstrate refractive index. The bulk sensitivity (BS) and FoM for each Fano resonance has been provided on the figure. (c) Transmittance spectra of the same HNH array as the thickness of an adlayer grows from zero to 14 nm. (d) Shift in the resonance wavelengths with respect to their nominal values for the case of no adlayer *vs*. the adlayer thickness. The surface sensitivity (SS) for each resonance has been provided on the figure. The inset to part (d) shows a sketch of the adlayer (black) assumed to form on the structure.

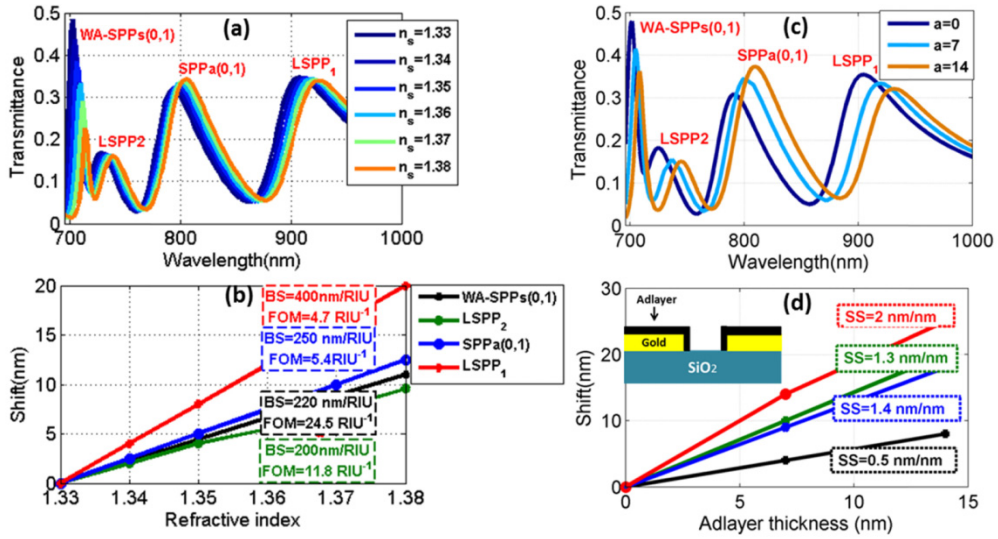

Fig. 9. Transmittance spectra of the HNH array illuminated with a z-polarized incident light, (a) while n_s changing. (b) Shift in the resonance wavelengths with respect to their nominal values at n_s = 1.33 *vs*. the superstrate refractive index. The bulk sensitivity (BS) and FoM for each resonance has been provided on the figure. (c) Transmittance spectra of the same HNH array as the thickness of an adlayer grows from zero to 14 nm. (d) Shift in the resonance wavelengths with respect to their nominal values for the case of no adlayer *vs*. the adlayer thickness. The surface sensitivity (SS) for each resonance has been provided on the figure. The inset to part (d) shows a sketch of the adlayer (black) assumed to form on the structure.

Optics EXPRESS

3.5.2 Surface sensitivity

Figure 8 (c) reveals how the Fano resonances red-shift with small changes in the adlayer thickness a (Δa = 7nm) for the case of y-polarized incident light. In a biosensing experiment the metal surface in contact with an aqueous sensing solution (cover) would be functionalized chemically to react selectively with a target analyte. As analyte binds, an adlayer of refractive index greater than the sensing solution forms, which shifts the resonance wavelengths. Here, the adlayer formation is modeled as a uniform dielectric layer of refractive index n_{ad} = 1.5 (which is typical of biochemical matter), growing from a thickness of a = 0 to 14 nm (in steps of 7 nm, due to discretization constraints), representing the accumulation of biomaterial on the gold surface, as sketched in the inset of Fig. 8 (d). As illustrated in Figs. 8 (c) and 8(d), increasing the adlayer thickness causes the resonances to red-shift, which results in surface sensitivities of 0.43, 1.43 and 2 nm/nm for the WA-SPP_s(1,0), SPP_a(1,0) and $LSPP_1$ Fano resonances, respectively. The highest surface sensitivity is produced by the $LSPP_1$ Fano resonance, because it has the highest field enhancement and confinement near the adlayer, compared to the other resonances. The WA-SPP_s(1,0) produces the lowest sensitivity because SPP_s modes (excited at Au/cover medium interface) exhibit the lowest field confinement to the interface, so less overlap with the adlayer. For z-polarized incident light, the evolution of the Fano resonances with small changes in the adlayer thickness is given in Figs. 9 (c), and 9 (d) shows the shift in the resonance wavelength with respect to their nominal values at a = 0 *vs*. the adlayer thickness. The surface sensitivity of each Fano resonance is also given.

4. Conclusions

In conclusion, we have studied theoretically and numerically the optical properties of arrays of heptamer arranged nanoholes in detail. The optical responses are influenced by various phenomena, such as LSPP excitations, diffractive effects, the excitation of propagating SPP modes on the metal film and of WA waves in either media, resulting in the formation of several pronounced Fano resonances, producing high transmittance (~50%) over the wavelength range investigated (630 to 1000 nm). To understand the physical mechanism behind the generation of each Fano resonance, electromagnetic near-field distributions were computed and presented, along with the effects of varying the geometrical parameters, such as the periodicity, metal thickness, inter-hole distance and diameter of the central hole. In addition, the grating dispersion equation was combined with modal computations of the symmetric and asymmetric SPP modes supported by the metal film (SPP_s, SPP_a) to further elucidate the origin of the resonances. We examined the structure for use as a biosensor by calculating the bulk and surfaces sensitivities, and FoM. The highest bulk (400 nm/RIU) and surface (2 nm/nm) sensitivities are produced by LSPP Fano resonances, whereas the highest FoM (24.5 RIU^{-1}) is obtained for the WA-SPP_s Fano resonance. Compared to the single nanohole arrays, this structure provides us with and improved bulk sensitivity, FoM values [48,56,57], and a higher transmittance (~50%) [40,48,58,59], while compared to its complementary structure, it shows a comparable sensitivity and FoM values [4]. However the spectrum of the HNH array is rich in features, which allows for a broadband interrogation and then improvement of the detection limit and measurement accuracy.

Funding

Natural Sciences and Engineering Research Council of Canada (NSERC) RGPIN-2016-04197); University of Ottawa Stephen Odoysk Memorial Scholarship (01476).

Acknowledgements

We would like to acknowledge the Centre for Advanced Computing (CAC), Queen's University, for the computational support, and also CMC Microsystems for the provision of COMSOL software that facilitated this research.